Serpentinization of oceanic peridotites: 1. A high-sensitivity method to monitor magnetite production in hydrothermal experiments

Benjamin Malvoisin, Julie Carlut, Fabrice Brunet

Serpentinization of oceanic peridotites: 1. A high-sensitivity method to monitor magnetite production in hydrothermal experiments

Benjamin Malvoisin,[1,2] Julie Carlut,[1,3] and Fabrice Brunet[1,2]

Received 22 June 2011; revised 10 November 2011; accepted 11 November 2011; published 21 January 2012.

[1] A new method using the magnetic properties of magnetite, Fe_3O_4, was developed to monitor experimental serpentinization. The saturation remanent magnetization signal (Jrs) was measured during the course of experiments designed to react San Carlos olivine, $(Mg_{0.91}, Fe_{0.09})_2SiO_4$, with water at 250 to 350°C and 500 bars. At the end of the experiments, the ratio with saturation magnetization (Jrs/Js ratio) allowed to convert each successive Jrs measurement into an in situ amount of magnetite produced by the serpentinization reaction. Water weight loss was also measured on the end product to determine the final degree of serpentinization. The application of this procedure to a series of experiments performed at 300°C/500 bars for various run duration (9 to 514 days) and starting olivine grain size (1 to 150 μm) shows a linear relationship between magnetite production and reaction progress. This relationship can be safely transposed to other experimental conditions using thermochemical modeling and/or the Fe content of the product phases. We show that this high-sensitivity magnetic method is a powerful tool to precisely monitor serpentinization kinetics in Fe-bearing systems. It represents, in addition, a new indirect mean for monitoring the production of hydrogen which is bound to magnetite production rate.

Citation: Malvoisin, B., J. Carlut, and F. Brunet (2012), Serpentinization of oceanic peridotites: 1. A high-sensitivity method to monitor magnetite production in hydrothermal experiments, *J. Geophys. Res.*, *117*, B01104, doi:10.1029/2011JB008612.

1. Introduction

[2] The formation of serpentine group minerals by hydration of ultramafic rocks occurs, extensively, in two main geological settings: (1) at slow spreading ridge where mantle-derived rocks are exposed tectonically on the seafloor to seawater alteration [*Cannat et al.*, 1992; *Cannat*, 1993] and (2) at the mantle wedge in subduction zones [*Hyndman and Peacock*, 2003] by reaction with aqueous fluids released by the downgoing slab. This exothermic transformation of olivine and pyroxene into magnetite and mechanically weak serpentine-group minerals induces major changes in the thermal structure, the magnetic properties and the rheology of both oceanic lithosphere and mantle [*Christensen*, 1966; *Fyfe*, 1974; *Toft et al.*, 1990; *Krammer*, 1990; *Escartín et al.*, 1997, 2001; *Oufi et al.*, 2002; *Brocher et al.*, 2003; *Emmanuel and Berkowitz*, 2006; *Delescluse and Chamot-Rooke*, 2008]. This reaction is a RedOx reaction involving oxidation of a part of the ferrous iron contained in the primary minerals coupled to the production of hydrogen by water reduction [*Neal and Stanger*, 1983; *Abrajano et al.*, 1990; *Charlou et al.*, 2002]. Iron is incorporated both as ferrous and ferric iron in hydrous phases and magnetite [*Moody*, 1976; *Evans*, 2008; *Marcaillou et al.*, 2011]. However, in natural systems, the distribution of trivalent iron between reaction products is complex and varies nonlinearly with the reaction progress. In particular, a peak of magnetite production is observed when the reaction reaches 60% completion [*Toft et al.*, 1990; *Oufi et al.*, 2002; *Bach et al.*, 2006]. Experiments and modeling by *Seyfried et al.* [2007] and *Klein et al.* [2009] suggest, in addition, that magnetite is only produced at temperatures above approximately 200°C and for a water to rock ratio below 50, trivalent iron being stored in serpentine otherwise. When magnetite is produced changes in magnetic properties of the rock are observed. While unreacted peridotites do not carry a significant magnetic signal, highly serpentinized peridotites carry a remanent magnetization because of their significant magnetite content [e.g., *Toft et al.*, 1990; *Oufi et al.*, 2002].

[3] Several authors have experimentally investigated the olivine + H_2O or peridotite + H_2O systems [*Martin and Fyfe*, 1970; *Moody*, 1976; *Berndt et al.*, 1996; *Seyfried et al.*, 2007; *Marcaillou et al.*, 2011], but while magnetite production during serpentinization in natural systems has being extensively studied [*Bina and Henry*, 1990; *Toft et al.*, 1990; *Nazarova*, 1994; *Oufi et al.*, 2002; *Liu et al.*, 2010], production during experiments has not attracted much attention. Monitoring magnetite formation during

[1]Laboratoire de Géologie, Ecole Normale Supérieure, CNRS, Paris, France.
[2]Maison des Géosciences, Université de Grenoble 1, ISTerre, CNRS, Grenoble, France.
[3]Laboratoire de Géosciences Marines, Institut de Physique du Globe de Paris, CNRS, Paris, France.

0148-0227/12/2011JB008612

Table 1. Experimental Conditions, Magnetic Properties, and Morphological Parameters of Magnetite

Run/ Reference	Temperature (°C)	NaCl	Initial Grain Size (μm)	Duration (h)	S[a] (%)	MFM[a] (mg)	Jrs[a] (10^{-6}.A.m^2)	Jrs/Js[a]	Hcr[a] (mT)	Hc[a] (mT)	Hcr/Hc	K[a] (SI)	D[a] (μm)	WMD[a] (μm)	E[a]	WE[a]	Mg (Brc)[a]	Mg (Srp)[a]
1	300		100–150	3500	<1[b]	0.2	1.38	0.0707	15.7	8	1.96	0.0014	N.D.	N.D.	N.D.	N.D.	N.A.	N.A.
2	300		50–63	12300	80	7.9	63.51	0.0874	33.4	11.67	2.862	0.0468	0.79	9.46	0.66	0.77	0.93 ± 0.02	0.98 ± 0.009
3	300	X	100–150	3400	<1[b]	0.2	1.71	0.0773	30.5	8.35	3.653	0.0013	N.D.	N.D.	N.D.	N.D.	N.A.	N.A.
5	300	X	0–38	1550	75	5	33.11	0.0721	33.1	10.05	3.294	0.0322	0.75	5.54	0.62	0.7	0.90 ± 0.02	0.97 ± 0.004
6	300		0–38	1260	5[c]	0.5	3.26	0.0758	55.1	10.06	5.477	0.0053	1.53	6.06	0.71	0.79	0.91 ± 0.02	0.97 ± 0.03
7	350		38–50	6220	1	0.2	1.05	0.0701	N.D.	11.4	N.D.	0.0016	1.3	2.45	0.65	0.68	N.A.	N.A.
8	350		38–50	2580	1	0.1	0.97	0.091	29.6	9.55	3.101	0.0008	0.92	1.65	0.73	0.8	N.A.	N.A.
10	300		38–50	6020	38	3.9	22.01	0.0619	38.5	9.52	4.044	0.0274	1.26	2.99	0.7	0.74	0.95 ± 0.01	0.98 ± 0.01
11	270		38–50	5960	32	3.3	17.71	0.0587	28.3	9.01	3.142	0.0203	1.04	3.37	0.7	0.77	0.93 ± 0.02	0.99 ± 0.01
12	250		38–50	5180	26	1	6.68	0.0765	18.4	8.84	2.081	0.0038	0.73	1.96	0.66	0.77	0.93 ± 0.04	0.98 ± 0.007
16	300		5–15	1800	30	3.4	23.81	0.0766	38	9.61	3.954	0.0202	0.55	5.27	0.67	0.72	0.92 ± 0.01	0.97 ± 0.01
17	300		5–15	215	8.5	0.7	5.18	0.0797	42.9	8.5	5.047	0.0052	0.57	2.23	0.66	0.67	N.A.	N.A.
20	300		5–15	1800	68	6.1	50.91	0.0914	35.7	11.36	3.143	0.039	0.78	4.92	0.65	0.72	0.93 ± 0.03	0.97 ± 0.01
21	300		5–15	600	18	1.8	12.21	0.0741	42.5	9.9	4.293	0.0097	0.8	2.57	0.63	0.61	0.92 ± 0.01	0.97 ± 0.03
22	300		5–15	1760	89	5.6	49.11	0.0951	39.7	12.27	3.236	0.0372	0.48	1.98	0.69	0.74	0.88 ± 0.02	0.96 ± 0.008
24	300		1–5	2390	91	9	66.11	0.0796	37	10.49	3.527	0.0707	0.34	2.65	0.73	0.75	0.92 ± 0.01	0.97 ± 0.004
25	270		5–15	1470	58	3.9	28.01	0.0778	34.5	10.44	3.305	0.0263	0.59	3.22	0.64	0.71	0.90 ± 0.03	0.96 ± 0.009
Antigorite												0.0005						
Lizardite												0.0004						
Chrysotile												0.0015						
Olivine SC							0.0004					0.0005						

[a]S, reaction progress determined from water weight loss; MFM, total mass of produced magnetite; Js, saturation magnetization; Jrs, saturation remanent magnetization; Hcr, remanent coercivity; Hc, intrinsic coercivity; K, susceptibility; D, mean diameter; WMD, D weighted by the surface mean diameter of magnetite; E, mean elongation ratio; WE, E weighted by the surface mean elongation ratio; Mg (Brc) and Mg (Srp), Mg/(Mg + Fe) ratio in brucite and in serpentine, respectively (errors were determined by taking the highest and the lowest values of a set of 5 to 17 measurements depending on the run); N.D., not determined; N.A., not analyzed.

[b]Estimation from backscattered electron images for experiments for which water incorporation is too low to be accurately determined with weight loss measurement.

[c]Reaction progress determined with infrared spectroscopy.

serpentinization experiments can provide new constraints on the serpentinization process and, in particular, on its kinetics. We have developed a high-sensitivity magnetic method to precisely monitor (1) the formation of magnetite and, indirectly, (2) the serpentinization rate of olivine. This method is based on the quantification of the amount of magnetite produced during the reaction between iron-bearing olivine and aqueous fluid under geologically relevant pressures and temperatures according to the following reaction:

$$\begin{aligned}\left(Mg,Fe^{2+}\right)_2SiO_4 + H_2O \rightarrow \left(Mg,Fe^{2+},Fe^{3+}\square\right)_3Si_2O_5(OH)_4 \\ + \left(Mg,Fe^{2+}\right)(OH)_2 + Fe^{3+}{}_2Fe^{2+}O_4 + H_{2,aq}.\end{aligned}$$

$$\text{olivine} + \text{water} \rightarrow \text{serpentine} + \text{brucite} + \text{magnetite} + \text{hydrogen} \quad (1)$$

[4] Methods to use the magnetic signal to monitor RedOx reactions have already been successfully applied to hydrothermal mineral systems [*Cairanne et al.*, 2003]. The saturation magnetization [*Moody*, 1976] and the susceptibility [*Seyfried et al.*, 2007] were also used to estimate the final amount of magnetite produced in serpentinization experiments. Here, the magnetic approach is extended to monitor reaction progress in the experimental charge, by combining (1) saturation remanent magnetization (Jrs) data on encapsulated samples, (2) the determination of the amount of water consumed by the reaction (weight loss on residual water evaporation) and (3) thermochemical modeling of the iron distribution among the serpentinization reaction products, namely, serpentine, brucite and magnetite.

2. Experimental and Analytical Methods

[5] Calibrated San Carlos olivine powders (Fo_{91}) with sizes ranging from 1 to 150 μm (dry sieving and/or Stokes' separation) were loaded in 2 to 3 cm length gold capsules (4.8 mm outer diameter and 4.4 mm inner diameter) together with deionized water (resistivity of 18 Ω.cm) or with an aqueous solution containing 33 g/L of NaCl, in a fluid/olivine mass ratio of approximately 2:5. The capsules, once filled, were welded shut and placed in a horizontal cold seal pressure vessel. The temperature of the experiments was between 250°C and 350°C and was measured with an external Ni-NiCr thermocouple and regulated to within 1°C (see the work of *Brunet and Chopin* [1995] for experimental details). A pressure of 500 bars was achieved in all experiments by pumping argon into the vessel. Overall, seventeen experiments were carried out (see Table 1 for parameters and results for each experiment).

[6] The serpentinization of Fe-bearing olivine is accompanied by the formation of magnetite, Fe_3O_4 [see, e.g., *Moody*, 1976, relation (1); *Evans*, 2008] which is ferrimagnetic and therefore can be monitored magnetically. Prior to each magnetic measurement, the sample capsule was quenched by cooling the vessel with a compressed air stream. Quench-measurement-loading cycles were repeated from every 2 days to every month depending on the kinetics of the reaction. Magnetic measurements were performed on the sample without opening the capsule (i.e., no fluid release). We collected isothermal remanent magnetization (IRM) curves by applying a magnetic field of 25, 50, 100, 150, 300, 500 and 1000 mT to the encapsulated sample and by measuring its remanent magnetization (Jrs) after each application (Figure 1). Two cross-checked cryogenic magnetometers (2G) were used at IPG (Paris) and ENS (Paris), respectively. In order to evaluate the noise signal, IRM was first measured on an empty gold capsule and on a gold capsule containing the starting olivine powder. The IRM was found to respectively reach 7.10^{-4} and

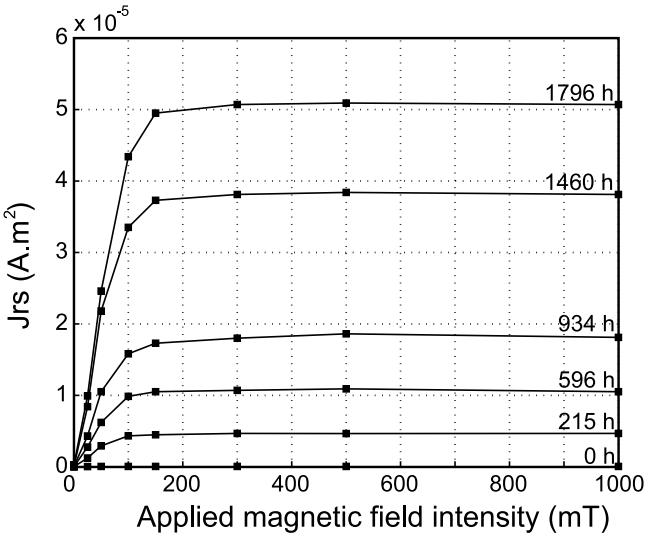

Figure 1. Isothermal remanent magnetization (IRM) acquisition curves on Run 20 (S = 68%) quenched at different time (from 0 to 1796 h). Note the increasing saturation remanent magnetization (Jrs) as time increases and the low coercivity of the produced magnetic phase.

3.10^{-2}% of the maximum Jrs measured in all the experiments. At the end of the serpentinization runs, which lasted from 9 days up to 514 days, a final magnetic measurement was performed before each capsule was opened and maintained at 110°C until all the remaining water was evaporated. The difference between the initial amount of water introduced in the capsule and the amount of residual water (given by the weight loss measurement) was assumed to correspond to the incorporation of water into the hydrous phase products (serpentine and brucite). The relationship between the proportion of hydrous phases (serpentine and brucite) and the serpentinization reaction progress depends, in particular, on the amount of iron incorporated into these products. The equilibrium iron distribution between serpentine, brucite and magnetite was calculated using the thermodynamic database of *Klein et al.* [2009] and the procedure described in Appendix A. Finally, the reacted powder was recovered and, the magnetic susceptibility and the hysteresis parameters were determined for each sample with a KLY-3 and a translation magnetometer at ENS (Paris) and IPGP (Saint Maur), respectively. Samples were further characterized using a field emission scanning electron microscope (FE-SEM, Zeiss Σigma™) equipped with a 50 mm^2 EDS detector (X-Max™ from Oxford Instrument), powder X-ray diffraction (Rigaku ultraX18HFCE in Bragg-Brentano geometry) and IR spectroscopy (Bruker Hyperion 3000 with a MCT detector at 4 cm^{-1}) in transmission mode. For a quantification of hydrous phase proportions, infrared spectra were normalized to the area of their Si-O peak and the area of their O-H peak was compared to one of the most reacted samples (reaction progress of 80% as estimated using water weight loss) to estimate a reaction progress relative to this reference sample. Part of the run product was embedded in epoxy, cut and polished for further FE-SEM characterization. In particular, the morphology of the magnetite grains was quantified by processing backscattered electron (BSE) images using the Matlab software. Images were binarized using the high brightness of magnetite in BSE mode with pixel sizes ranging from 0.15 × 0.15 μm^2 to 0.3 × 0.3 μm^2. The morphology of magnetite grains was defined by an elongation parameter, **b**/**a**, which was obtained by fitting the grain to an ellipse (**a**: long semiaxis and **b**: short semiaxis). The size and the surface area of the grain sections were measured to obtain a mean diameter and a weighted mean diameter (WMD) for each experiment. The WMD represents the average apparent diameter weighted by the contribution of each grain to the total magnetite volume (i.e., to the magnetic signal):

$$WMD = \frac{\sum_j (d_j \cdot s_j)}{\sum_j s_j}$$

where d_j and s_j are, respectively, the diameter and the surface of the given grain section (Table 1). $\sum_j s_j$ and $\frac{s_j}{\sum_j s_j}$ represent the whole magnetite volume and the contribution of each grain to this volume, respectively. The same formalism was used to calculate a weighted mean elongation (WE).

3. Results

3.1. Evolution of the Magnetic Signal

[7] IRM is found to increase for all samples when the reaction proceeds (Figure 1). This is an indication that a magnetic mineral is created in the course of the hydrothermal experiments. In addition, this magnetic mineral is of low coercivity since the samples are saturated by 300 mT (Figure 1). There is no evolution of the shape of the IRM curve with the duration of the serpentinization experiments, only an increase in the intensity of the measured Jrs is observed.

3.2. Nature and Morphology of the Iron Oxide

[8] Powder X-ray diffraction and FE-SEM inspection allowed the identification of serpentine, brucite and iron oxide which all coexist with residual olivine, in the run products. The serpentine polymorph present was identified with micro-Raman spectroscopy as being predominantly lizardite. An ambiguity remained however on the exact nature of the iron oxide(s), magnetite and/or maghemite, the presence of both of which being compatible with the low coercivity observed on the IRM curve (Figure 1). In order to lift this ambiguity, we measured the thermomagnetic curve (collected in a nitrogen atmosphere, Figure 2) for a highly reacted sample (Run 2; S = 80%; Table 1). This curve is mostly reversible and provides a Curie temperature of 592°C (obtained using the differential method proposed by *Tauxe* [1998]). These two features are typical for pure magnetite and allow unambiguous identification of the iron oxide as magnetite. The cooling curve shows the subtle contribution, starting at approximately 450°C, of a secondary phase which was produced upon heating; a likely explanation is that this phase could be a Mg-substituted magnetite formed from brucite and/or serpentine thermal decomposition.

[9] Electron microscope observations show that isolated magnetite grains (around 1 μm across) are found in all experiments. In addition, experiments with the smallest starting olivine grains (1–5 μm and 0–38 μm) produced homogeneous subhedral magnetite with sizes in the order of 5 μm (Figures 3a and 3b) whereas larger olivine grain sizes (more than 5 μm)

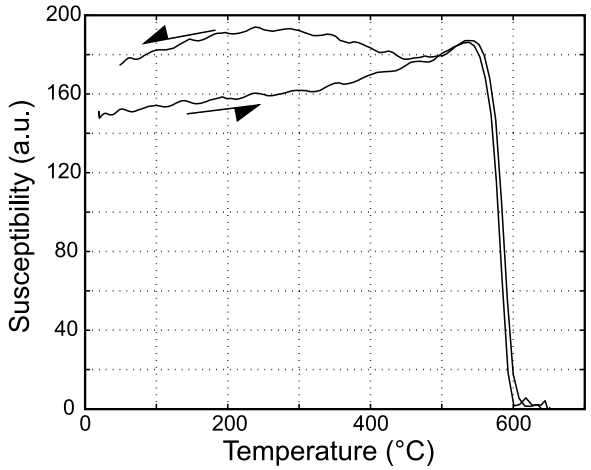

Figure 2. Thermomagnetic curve for Run 2. Heating and cooling stages are indicated with arrows. This curve indicates magnetite as magnetic signal carrier with a Curie temperature of 592°C. Upon cooling, another magnetic phase, which probably formed during heating, contributes to the signal from 450°C and below.

produced magnetite aggregates or sieve-textured grains, some of them up to 20 μm across (Figures 3c and 3d).

[10] For each experiment, BSE image analysis on polished sections indicates a mean apparent magnetite diameter (D) of 0.8 $\pm$ 0.5 μm for grains (or aggregates) with size above 300 nm, i.e., close to the SEM resolution (D, Table 1). The WMD was retrieved (see experimental and analytical methods). WMD ranges from 1.65 μm (Run 8) to 9.5 μm (Run 2) falling within the range of pseudo-single-domain (PSD) to multidomain (MD) magnetite grain sizes [*Day et al.*, 1977; *Dunlop*, 1981]. With mean elongations ranging from 0.62 to 0.73, magnetite grains do not show a strong shape anisotropy (Table 1) able to influence the magnetic signal [*Özdemir and Dunlop*, 1992]. When it is weighted to the volume contribution of each grain, elongation is systematically higher (0.67 to 0.77); large grains are thus less elongated than small grains as shown by SEM observation. Apart from the difference in texture, there is no clear relationship between morphological parameters of magnetite, including crystal size, and any experimental parameters (reaction progress, duration, initial olivine grain size, etc.).

3.3. Hysteresis Parameters and Texture Observation of the Produced Magnetite

[11] Hysteresis parameters were acquired to determine the amount of magnetite in each sample using the saturation

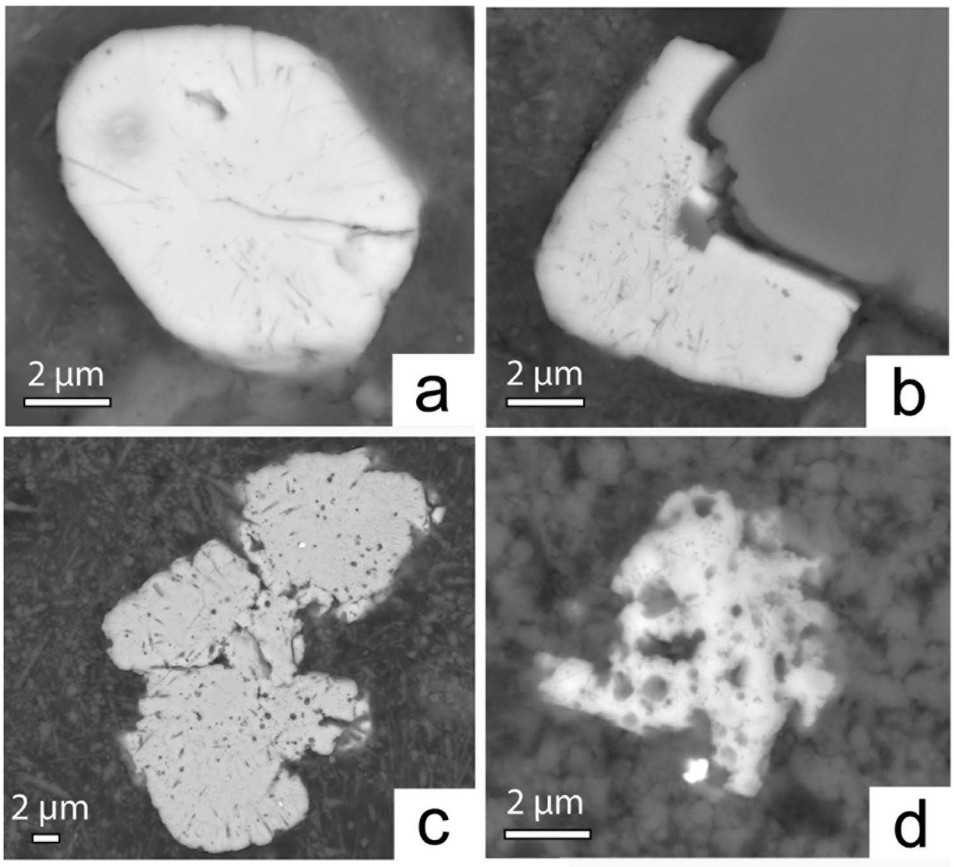

Figure 3. Backscattered electron images of magnetite grains from (a and b) Run 6 and (c and d) Run 2. Note the differences of morphology with homogeneous grains (Figures 3a and 3b) and aggregates of grains or porous-like grains (Figures 3c and 3d). The bright spot on Figure 3d is an Fe-Ni alloy only observed in this experiment (reaction product or contamination?).

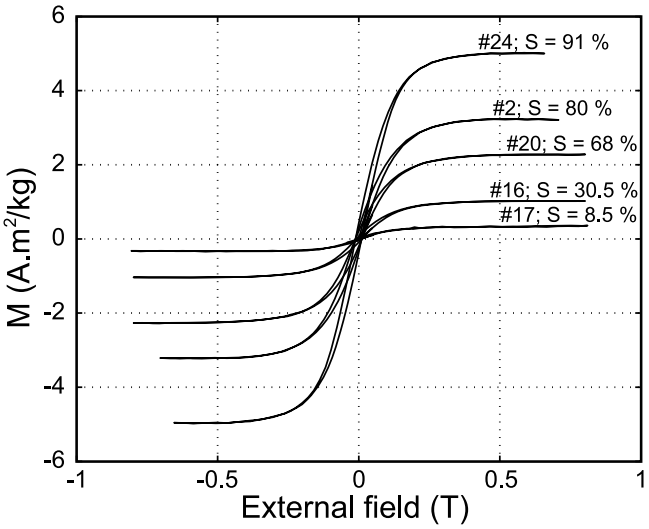

Figure 4. Hysteresis loops of run products obtained at 300°C/500 bars. Both Js (saturation of the hysteresis) and Jrs (at the intersection between hysteresis loops and *y* axis, not shown) increase with the extent of serpentinization (S).

magnetization and to characterize the domain structure of the produced magnetite. Calibration between Js and amount of magnetite was investigated by measuring Js of powder mixtures containing olivine (synthetic forsterite) with 1, 3, 6 and 10 wt.% of synthetic magnetite (M-10T from Rana Gruber (Norway)). A correlation factor of 0.999 and a proportionality factor of 92 A.m^2/kg were obtained between Js and the nominal weight of magnetite in excellent agreement with previous studies [*O'Reilly*, 1984].

[12] Typical hysteresis diagrams acquired on end products are shown on Figure 4. Jrs/Js ratio (0.059–0.095) and Hcr/Hc ratio (2.0–5.5) are both indicative of magnetite grains with a domain structure lying at the boundary between PSD and MD [*Stoner and Wohlfarth*, 1948; *Rahman et al.*, 1973; *Day et al.*, 1977; *Dunlop*, 1981; *Dunlop*, 2002]. These results are in agreement with the SEM observations. The dependence of Jrs/Js and Hc on mean magnetite grain size (calculated using the WMD), of Js on susceptibility and of susceptibility on Hcr/Hc (Figure 5) shows that magnetite in our samples is, in general, closer to crushed grains (CG), i.e., with induced "crystal defects" [*Day et al.*, 1977], rather than to precipitated grains (PG) [*Heider et al.*, 1987, 1996]. The presence of

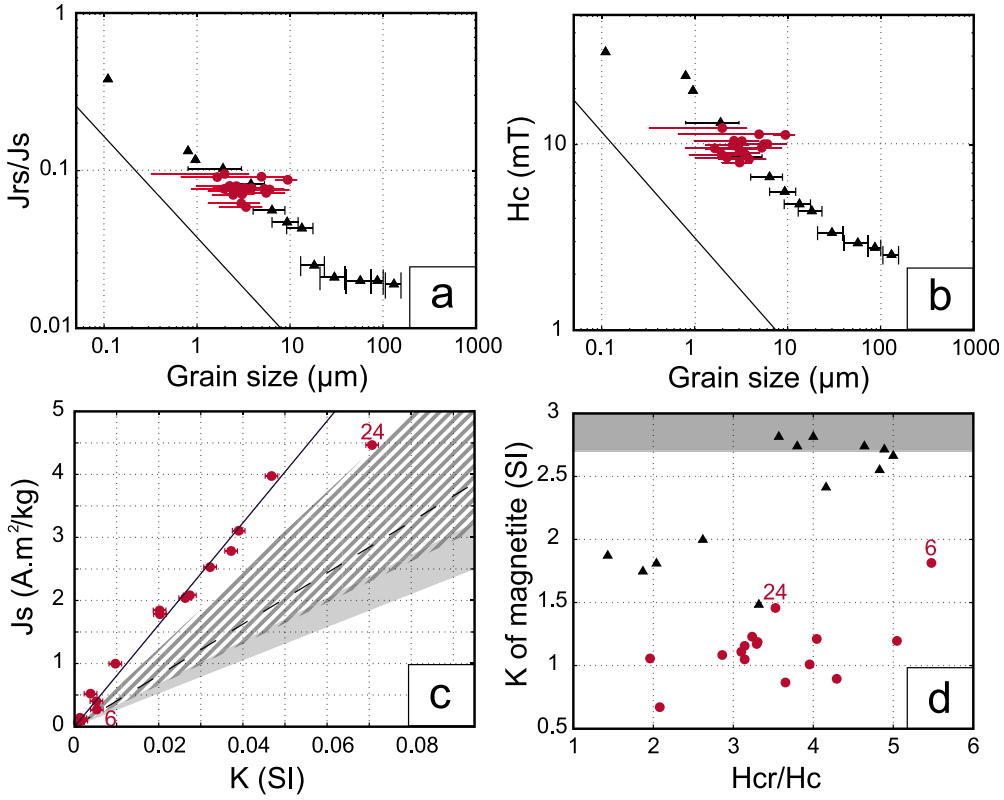

Figure 5. Comparison between the magnetic properties of the magnetite grains from our experiments and (red closed circle) with those of precipitated magnetite (straight line in Figures 5a and 5b and grey region in Figures 5c and 5d [*Heider et al.*, 1987, 1996]) and of crushed magnetite (triangles in Figures 5a, 5b, and 5d and hatched region in Figure 5c [*Day et al.*, 1977]). (a) Comparison of Jrs/Js ratio as a function of grain size. (b) Comparison of Hc as a function of grain size. Note the good agreement between properties measured here and those of crushed grains. (c) Js as a function of K. The plain draw line corresponds to a fit to our experiments whereas the dashed line is the same fit obtained for abyssal peridotites [*Oufi et al.*, 2002]. (d) K of magnetite as a function of the Hcr/Hc ratio. K of magnetite is calculated by removing the bulk effect due to the mixing with serpentine and brucite which are considered to have little effect on the susceptibility as suggested by measurements on natural chrysotile, antigorite and lizardite (Table 1).

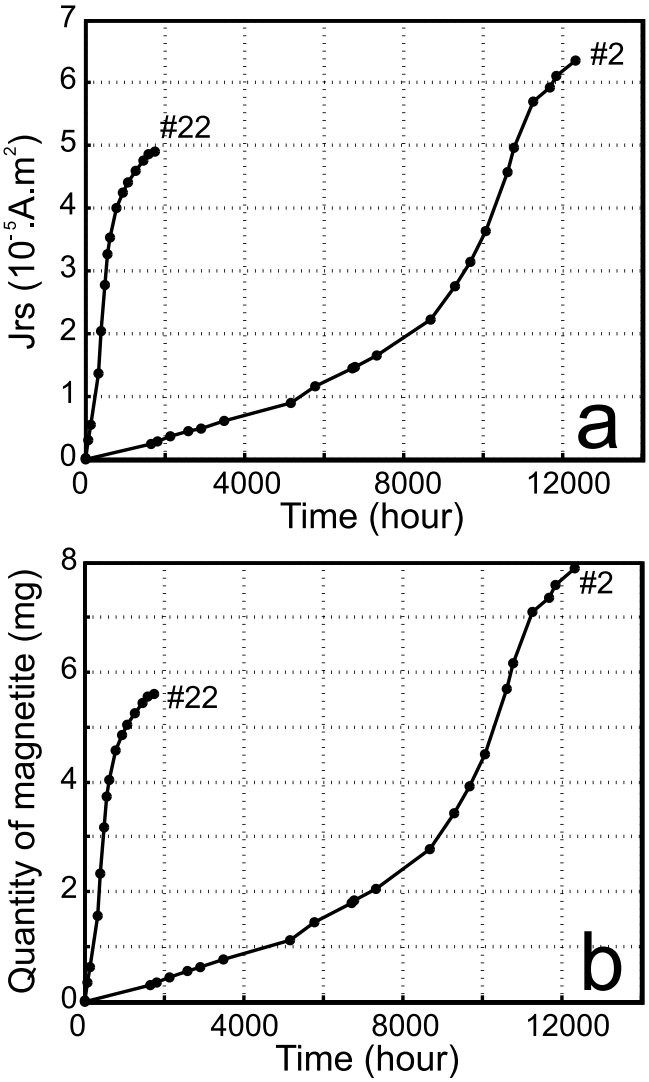

Figure 6. (a) Jrs as a function of time for Run 22 and Run 2 (300°C/500 bars) with an initial olivine grain size of 5–15 μm and 50–63 μm, respectively. (b) Same as Figure 6a but plotting the derivation of the amount of magnetite produced using Jrs/Js measurements.

crystal defects in magnetites produced in our experiments may be linked to the sieve texture of most of the grains observed by SEM (Figure 3).

[13] A deeper look at the results reveals that two runs with the smallest initial grain size (Run 6 (0–38 μm) and Run 24 (1–5 μm)) present slightly distinct magnetic parameters. As observed for natural peridotites [*Oufi et al.*, 2002], the magnetic data are characterized by a constant K/Js ratio (Figure 5c). However, Run 6 and Run 24 have a distinct K/Js ratio which is higher than that of the other experiments. In addition, the plot of susceptibility (K) as a function of Hcr/Hc (Figure 5d) shows again a distinct behavior for Run 6 and Run 24 which display the highest K and high Hcr/Hc ratios. Since the susceptibility measured on CG (as low as 1.5 S.I. [*Day et al.*, 1977]) is lower than that measured on PG (3.1 $\pm$ 0.4 S.I. [*Heider et al.*, 1996], Figure 5d), magnetites in Run 6 and Run 24 are the closest to PG. BSE images (Figure 3) of these two later samples showed that magnetite grains are mostly subhedral with little to no sieve texture, in contrast with magnetite grains produced in the other experiments. *Hu et al.* [2010] have shown that the habitus of precipitated magnetite depends on supersaturation level; at high degree of supersaturation, octahedral morphology is obtained whereas, at low degree of supersaturation, sheet-like crystals are formed. This may indicate that a relatively high level of magnetite supersaturation was achieved for the smaller initial olivine grain size (<5 μm) because of faster dissolution.

4. Discussion

4.1. From the Remanent Saturation Magnetization to the Amount of Magnetite

[14] Hysteresis parameters could not be measured on the encapsulated quenched samples for technical reasons (improper size of the gold capsule and lack of cohesion of the olivine grains in the capsule). They were thus only measured, for each experiment, after the sample powder was extracted from the capsule. Instead, we measured Jrs, the remanent saturation magnetization, which is also related to the magnetite content (Figure 6a). However, Jrs is also sensitive to the magnetite size distribution. In particular, the smallest grains in the superparamagnetic state, with sizes on the order of 10 nm or less, have a low relaxation time, typically less than a few tens of seconds [*Néel*, 1953] and thus cannot be detected by this approach. Consequently, Jrs/Js ratio derived from hysteresis loops, collected at the end of each experiment, were used in order to convert Jrs into Js. Jrs/Js ratios were found to be very homogenous: more than half of the samples have Jrs/Js values comprised between 0.07 and 0.08, the whole range being comprised between 0.059 (Run 11) and 0.095 (Run 22). In addition, the Js/Jrs ratio is found to be independent of the duration of the experiments and thus, independent of reaction progress. The Js/Jrs ratio determined at the end of each experiment can thus be used to safely convert each time-resolved Jrs measurement into a Js value in order to derive time-resolved magnetite contents. However, the accuracy of the magnetite content estimate depends on resolution limits of the magnetic signal. Since the sensitivity of the cryogenic magnetometer is of 10^{-11} A.m^2, the magnetite detection threshold will be limited by the noise level of the experiment, i.e., in the present case, the magnetic signal of the unreacted gold capsule loaded with olivine (5.10^{-8} A.m^2). Converting this signal into a molar percentage yields a very low detection limit of 30 ppm of magnetite allowing accurate estimate even for low reaction progress. As an illustration, Figure 6b shows how the amount of magnetite produced, at 300°C/500 bars, when plotted as a function of time, displays a well define sigmoid curve.

4.2. From Amount of Magnetite to Reaction Progress

[15] The link between amount of magnetite and progress of the olivine serpentinization reaction was investigated through a batch of ten experiments (referred to as Batch300 in the following) run under identical conditions (300°C/500 bars, deionized water) but with different initial grain sizes and quenched at different time. Reaction progress was estimated from the amount of water incorporated in reacting phases quantified in two ways, using water weight loss upon evaporation, and through the amount of produced hydrous

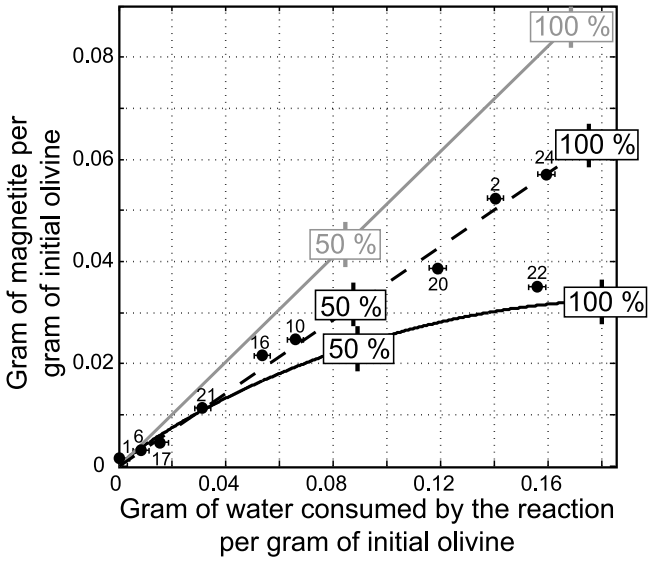

Figure 7. Mass of magnetite produced at 300°C/500 bars (deionized water) as a function of the mass of water incorporated in the hydrous minerals. Each data point is labeled with the corresponding run number. Simulation results are also represented: Model 1 (gray line), Model 2 (black line,) and Model 3 (dashed line).

phases (brucite and lizardite) as determined using infrared spectroscopy. Both measurements were found to be in good agreement with a correlation factor of 0.98. Infrared spectroscopy is very sensitive to the presence of serpentine with an O-H peak observed for experiments having reacted to less than 1%. Because of weighing uncertainty, the accuracy on reaction progress inferred from water weight loss is estimated to approximately ±2%. Repeated measurements performed on the same powder showed that the precision of the spectroscopic data varies from approximately ±5% to approximately ±10% for reaction progresses of 25% and 70%, respectively. Consequently, the weight loss technique was preferred regarding the range of reaction extent investigated here, even though the relationship between water weight loss and reaction progress is not as straightforward as with IR spectroscopy (see below).

[16] In Figure 7, the amount of magnetite calculated from Js for each experiment is compared with the amount of water incorporated in the hydrous phases as derived from weight loss data. This comparison mostly shows a linear trend with the exception of one outlier point (Run 22). As already emphasized, the relationship between weight loss and reaction progress depends on the partitioning of iron between the reaction products. Indeed, ignoring the possible presence of Fe^{3+} in serpentine [*Evans*, 2008], the serpentinization of Fe-bearing olivine can be written as follows:

$$2(Mg_{1-x}Fe_x)_2SiO_4 + A\,H_2O = \left(Mg_{1-y}Fe_y\right)_3Si_2O_5(OH)_4 + B(Mg_{1-z}Fe_z)(OH)_2 + CFe_3O_4 + DH_2 \quad (2)$$

with $B = (1 - 4x + 3y) / (1 - z)$; $C = (4x - 3y - Bz)/3$; $A = 1 + 2B + 4C$ and $D = A - 2 - B$.

It can be seen from equation (2) that the water consumed by the reaction (and the hydrogen production rate), according to the *A* coefficient, is a function of the initial iron content in olivine as well as of the iron content in both brucite and serpentine.

[17] The end-member case (Model 1) where all the iron would be hosted by magnetite (i.e., y = z = 0 in equation (2)) is also plotted in Figure 7. It can be seen that the magnetite – reaction progress relationship determined experimentally significantly departs from this end-member case (Model 1) because or the presence of iron in brucite and/or lizardite. This observation prompted to a more sophisticated approach of the partition of iron between the products through thermochemical modeling (Model 2, Figure 7).

[18] The modal and chemical compositions of the run products were computed following the approach and the selected data detailed in Appendix A, at 300°C/500 bars. Possible incorporation of trivalent iron in serpentine was considered in this calculation. Reaction progress was simulated by stepwise changes of the reactant/water mass ratio from 0 (0% reaction) to 0.367 (100% reaction). At each step, the system becomes more reduced (i.e., higher H_2 activity) because of an increasing amount of produced magnetite, see relation (2). Therefore, the distribution of iron between brucite, serpentine and magnetite changes as a function of reaction progress (Figure 7, Model 2). As shown on Figure 7, Model 2 does not reproduce the linear relationship between magnetite production and reaction extent inferred from weight loss data. It appears that the best fit to the experimental data is obtained for a constant H_2 concentration set to approximately 0.13 mol/L (Figure 7, Model 3). The concentration in hydrogen of Model 3 was then used to derive the coefficient which relates serpentinization reaction progress and water incorporation in lizardite and brucite (or total water weight loss) for experiments run at temperatures different from 300°C (Figure 7). Overall, at the end of each experiment, the coefficient which relates reaction progress and magnetite content is established by (1) measuring the water weight loss, (2) by knowing the total amount of produced magnetite (Js) and (3) by retrieving the factor between water weight loss and reaction progress using Model 3. If reaction progress is retrieved with either Model 1 or Model 2 (the two end-member cases, Figure 8a), maximum differences by only 6% in the reaction progress estimate at the end of the experiment are reached (at 100% of reaction).

[19] In addition, the iron content of brucite and serpentine has been measured using EDS (Table 1). Mg/(Mg + Fe) ratios of 0.93 ± 0.02 and 0.98 ± 0.02 for brucite and serpentine, respectively, were obtained; this is fully consistent with the values calculated with Model 3, i.e., 0.94 and 0.97, respectively, giving confidence in our thermochemical model.

[20] Finally, in order to further investigate the link between magnetic parameters and the serpentinization reaction progress (S), Jrs, Js and K values obtained for Batch300 are plotted as a function of S (Figures 8b and 8c). K and both Js and Jrs appear to be proportional to the reaction progress over the whole range of reaction extent. This (1) graphically confirms that the ratio between Js and Jrs is roughly constant irrespective of the reaction progress and (2) shows that the magnetite production (proportional to Js) varies also linearly with the reaction progress. Compilation of magnetic data derived from abyssal peridotites and ophiolitic massifs samples [*Toft et al.*, 1990; *Oufi et al.*, 2002] shows that in

natural samples the amount of magnetite is generally not linearly related to serpentinization rate but increases exponentially with serpentinization degree (Figure 8c). *Toft et al.* [1990] interpret this as related to a reaction sequence with iron being first sequestrated in Fe-rich serpentine and brucite, two minerals which would then break down at higher serpentinization degree to form magnetite. *Bach et al.* [2006] proposed that the breakdown of ferroan brucite is due to an increase in $SiO_{2,aq}$ activity. We have shown here that magnetite production rate varies with temperature and H_2 activity during serpentinization. The variations of these conditions might also be a source of the exponential relationship observed in nature.

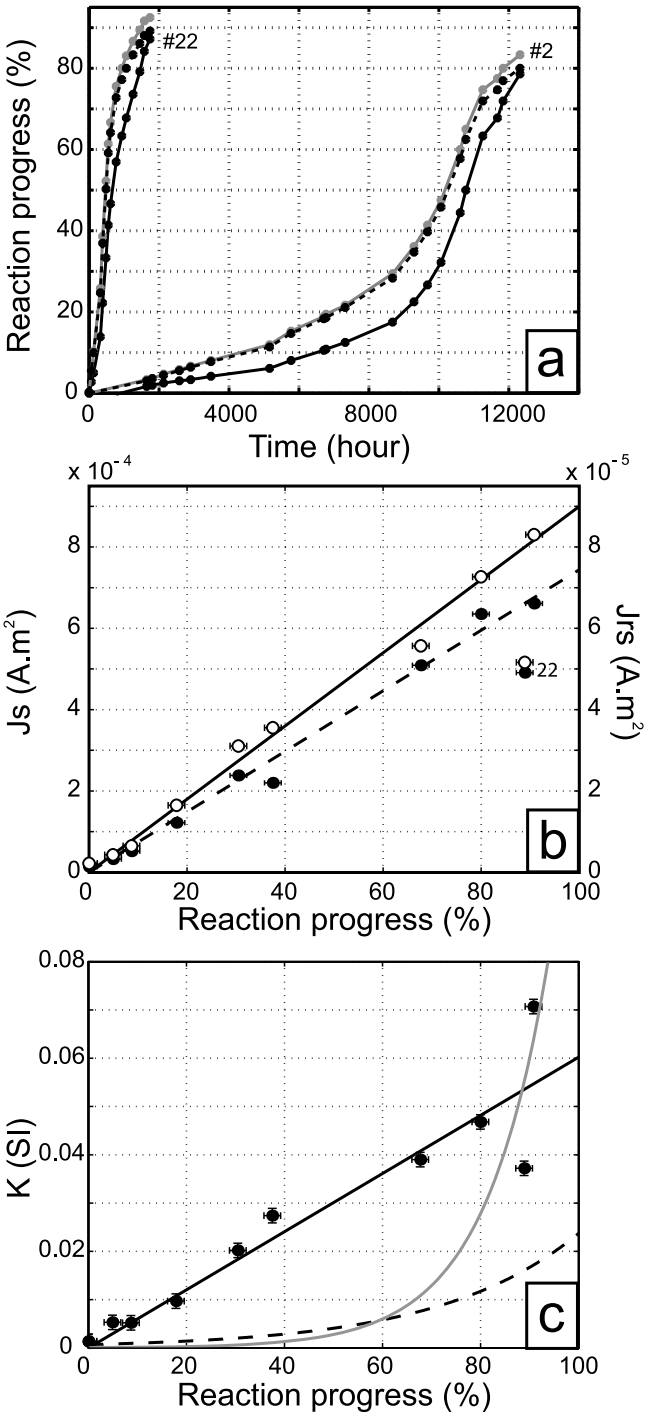

Figure 8. Relationship between reaction progress and time (Figure 8a) or magnetic parameters (Figures 8b and 8c) for Run 22 and Run 2 (Figure 8a) and for all the experiments conducted with deionized water at 300°C and 500 bars (Figures 8b and 8c). (a) Reaction progress inferred from the amount of produced magnetite. Dashed line is the reaction progress deduced from the model best fitting the data (Model 3). Black line corresponds to a reaction progress estimated using Model 2. Grey line refers to a reaction where all the iron would be incorporated into magnetite (Model 1, see text for details). (b) Js (open circles) and Jrs (closed circles) with their fit (plain and dashed lines, respectively) as a function of the reaction progress. Error bars on Jrs and Js are smaller than the size of the symbol. (c) Susceptibility (K) as a function of the reaction progress. Corresponding data for natural peridotites are from the work of *Toft et al.* [1990] (dashed line) and *Oufi et al.* [2002] (gray line).

4.3. Extension to Various Pressures and Temperatures and H_2 Behavior

[21] Reaction progress can be inferred from magnetite production at conditions different from 300°C and 500 bars only if (1) the relationship between magnetite content and reaction progress at the end of the reaction (written M/S in the following) is determined and if (2) the proportionality between reaction progress and magnetite production observed at 300°C/500 bars is still valid. Ratio M/S of 0.030, 0.065, 0.070, 0.13 mg per reaction percent for approximately 160 mg of initial olivine were obtained for run temperatures of 250, 270, 300 and 350°C, respectively (Table 1). M/S is found to increase with temperature because, as predicted by Model 3 and as already pointed out in previous studies [*Seyfried et al.*, 2007; *Klein et al.*, 2009; *Marcaillou et al.*, 2011], iron incorporation into magnetite is favored when temperature increases. The application of the method to various pressures and temperatures also requires that iron partitioning remains reaction-progress independent in that P-T range as observed at 300°C and 500 bars. This condition is met if RedOx conditions do not significantly change with reaction progress (see the assumption of constant H_2 activity in Model 3). The constant H_2 activity inference is somehow striking since it does not fit to the scheme of progressive water reduction as a response to magnetite production (Model 2). Possible H_2 leakage that would rapidly maintain the oxygen fugacity to a constant value is ruled out by the very low hydrogen permeability of gold below 350°C [*Chou*, 1986]. A more likely explanation would be that H_2 saturation in water is rapidly reached to form a H_2 gas phase which would then ensure a near constant H_2 activity in the aqueous solution. It is hardly possible to model equilibria involving gaseous phases because of the lack of H_2 solubility data at high pressure and high temperature as well as our poor knowledge of the nature of the possible gas phases inherited from the sample preparation stage. To give an indication, considering the end-member case where no H_2 gas is produced at all (i.e., highest possible

H_2 activity in the water; Model 2), instead of Model 3 (i.e., constant H_2 concentration set to 0.13 mol/L) to infer the reaction progresses (S), will give differences by 10% at most for S (Figure 8a). More importantly, the shape of the reaction progress – time curve and therefore the interpretation of the kinetics data, which are discussed in the companion paper (B. Malvoisin, Serpentinization of oceanic peridotites: 2. Kinetics and processes of San Carlos olivine hydrothermal alteration, submitted to *Journal of Geophysical Research*, 2012), would not be significantly affected.

5. Concluding Remarks

[22] The use of magnetic measurements to monitor the hydrothermal alteration of Fe-bearing olivine is an attractive method for the following reasons: 1. The extent of reaction can be determined without opening the capsule. 2. Magnetic measurement is very sensitive to reaction progress (S) compared to other characterization techniques such as XRPD or spectroscopy. Combining reasons 1 and 2, magnetic measurement is particularly appropriate to investigate in situ serpentinization kinetics on relatively small samples through time-resolved measurements (companion paper, B. Malvoisin, submitted manuscript, 2012). 3. Ferric iron concomitantly produced with dihydrogen is either incorporated into serpentine or in magnetite during serpentinization [*Evans*, 2008]. However, at temperature above 200°C, numerical and experimental studies [*Seyfried et al.*, 2007; *Klein et al.*, 2009; *Marcaillou et al.*, 2011] show that ferric iron is predominantly incorporated into magnetite. Consequently, magnetite production can potentially be used as a proxy for H_2 production. On the basis of thermochemical computation at 300°C/500 bars, it is estimated that 91% of the total H_2 produced by San Carlos olivine hydration is related to magnetite production. On the basis of this calculation and from the final mass of magnetite derived from the magnetic measurements, 0.044 mol of H_2 per mole of olivine has been produced at 300°C/500 bars in our experiments.

Appendix A

[23] To model the fO_2 evolution during olivine pure water interactions, the SUPCRT92 database [*Johnson et al.*, 1992] was complemented by thermodynamic data for greenalite, $Fe_3Si_2O_5(OH)_4$, "ferroan brucite," $Fe(OH)_2$, and Fe^{3+} serpentine, $Fe_2Si_2O_5(OH)_4$ [*Klein et al.*, 2009]. Because of the lack of thermodynamic data for lizardite which is mainly observed in our samples, chrysotile is used instead in the calculation. Note that thermodynamic data for greenalite were also derived by *Rasmussen et al.* [1998].

[24] Equilibration of a serpentinite with a fluid can be written as follows:

$$a\left(Mg_xFe_yFe_{2/3(1-x-y)}\right)_3Si_2O_5(OH)_4 + b\left(Mg_wFe_{(1-w)}\right)(OH)_2 + cFe_3O_4 + dH_2O \rightarrow e\left(Mg_xFe_yFe_{2/3(1-x-y)}\right)_3Si_2O_5(OH)_4 + f\left(Mg_wFe_{(1-w)}\right)(OH)_2 + gFe_3O_4 + hH_2O + iH_2, aq.$$

Once equilibrium is reached, four reactions describe the system: $H_2O = H_2,aq + 1/2O_2,aq$ (water dissociation); $Fe^{2+}{}_3Si_2O_5(OH)_4 + 3\ Mg(OH)_2 = Mg_3Si_2O_5(OH)_4 + 3\ Fe(OH)_2$ (Fe-Mg exchange between serpentine and brucite); $3\ Fe(OH)_2 = Fe_3O_4 + 2\ H_2O + H_2,aq$ (Fe-brucite oxidation coupled to water decomposition); $3\ Fe^{2+}{}_3Si_2O_5(OH)_4 + 4\ H_2O = 3\ Fe^{3+}{}_2\square Si_2O_5(OH)_4 + Fe_3O_4 + 4\ H_{2,aq}$ (Fe-serpentine oxidation coupled to water decomposition).

[25] This system of equations along with those of mass conservation is solved to determine the stable assemblage at fixed pressure and temperature. Results of our model were tested against the results of the models by *McCollom and Bach* [2009] and *Klein et al.* [2009] and were found to be in good agreement. (Even if, admittedly, a ferri-Tschermak's (cronstedite) solution is more common in serpentinite than the octahedral-vacancy solution used in this equation [e.g., *Evans*, 2008, Figures 3 and 6]).

[26] **Acknowledgments.** This research was funded by INSU-CNRS through the "Hydrogène Naturel" program. The authors thank M. Cannat for fruitful discussions. G. Montes-Hernandez is acknowledged for his help with the infrared spectrometer located at IPAG (Université J. Fourier, Grenoble). We thank N. Findling and M. Legoff for their help at using the FE-SEM (ENS, Paris) and the translation magnetometer (IPGP–St. Maur), respectively. This is IPGP contribution 3240.

References

Abrajano, T. A., N. C. Sturchio, B. M. Kennedy, G. L. Lyon, K. Muehlenbachs, and J. K. Bohlke (1990), Geochemistry of reduced gas related to serpentinization of the Zambales ophiolites, Philippines, *Appl. Geochem.*, *5*, 625–630, doi:10.1016/0883-2927(90)90060-I.

Bach, W., H. Paulick, C. J. Garrido, B. Ildefonse, W. P. Meurer, and S. E. Humphris (2006), Unraveling the sequence of serpentinization reactions: Petrography, mineral chemistry, and petrophysics of serpentinites from MAR 15°N (ODP Leg 209, Site 1274), *Geophys. Res. Lett.*, *33*, L13306, doi:10.1029/2006GL025681.

Berndt, M. E., D. E. Allen and W. E. Seyfried (1996), Reduction of CO_2 during serpentinization of olivine at 300°C and 500 bar, *Geology*, *24*, 351–354, doi:10.1130/0091-7613(1996)024<0351:ROCDSO>2.3.CO;2.

Bina, M. M., and B. Henry (1990), Magnetic properties, opaque mineralogy and magnetic anisotropies of serpentinized peridotites from ODP Hole 670A near the Mid-Atlantic Ridge, *Phys. Earth Planet. Inter.*, *65*, 88–103, doi:10.1016/0031-9201(90)90078-C.

Brocher, M., T. Parsons, A. M. Tréhu, C. M. Snelson, and M. A. Fisher (2003), Seismic evidence for widespread serpentinized forearc upper mantle along the Cascadia margin, *Geology*, *31*, 267–270, doi:10.1130/0091-7613(2003)031<0267:SEFWSF>2.0.CO;2.

Brunet, F., and C. Chopin (1995), Bearthite, $Ca_2Al(PO_4)_2OH$: Stability, thermodynamic properties and phase relations, *Contrib. Mineral. Petrol.*, *121*, 258–266, doi:10.1007/BF02688241.

Cairanne, G., F. Brunet, J.-P. Pozzi, P. Besson, and C. Aubourg (2003), Magnetic monitoring of hydrothermal magnetite nucleation-and-growth: Record of magnetic reversals, *Am. Mineral.*, *88*, 1385–1389.

Cannat, M. (1993), Emplacement of mantle rocks in the seafloor at mid-ocean ridges, *J. Geophys. Res.*, *98*, 4163–4172, doi:10.1029/92JB02221.

Cannat, M., B. Bideau and H. Bougault (1992), Serpentinized peridotites and gabbros in the Mid-Atlantic Ridge axial valley at 15°37′N and 16°52′N, *Earth Planet. Sci. Lett.*, *109*, 87–106, doi:10.1016/0012-821X(92)90076-8.

Charlou, J. L., J. P. Donval, Y. Fouquet, P. Jean-Baptiste, and N. Holm (2002), Geochemistry of high H_2 and CH_4 vent fluids issuing from ultramafic rocks at the Rainbow hydrothermal field (36°14′N, MAR), *Chem. Geol.*, *191*, 345–359, doi:10.1016/S0009-2541(02)00134-1.

Chou, I.-M. (1986), Permeability of precious metals to hydrogen at 2 kb total pressure and elevated temperatures, *Am. J. Sci.*, *286*, 638–658, doi:10.2475/ajs.286.8.638.

Christensen, N. I. (1966), Elasticity of ultrabasic rocks, *J. Geophys. Res.*, *71*, 5921–5931, doi:10.1029/JZ071i024p05921.

Day, R., M. D. Fuller, and V. A. Schmidt (1977), Hysteresis properties of titanomagnetites: Grain size and composition dependence, *Phys. Earth Planet. Inter.*, *13*, 260–267, doi:10.1016/0031-9201(77)90108-X.

Delescluse, M., and N. Chamot-Rooke (2008), Serpentinization pulse in the actively deforming Central Indian Basin, *Earth Planet. Sci. Lett.*, *276*, 140–151, doi:10.1016/j.epsl.2008.09.017.

Dunlop, D. J. (1981), The rock magnetism of fine particles, *Phys. Earth Planet. Inter.*, *26*, 1–26, doi:10.1016/0031-9201(81)90093-5.

Dunlop, D. J. (2002), Theory and application of the Day plot (M_{rs}/M_s versus H_{cr}/H_c) 1. Theoretical curves and tests using titanomagnetite data, *J. Geophys. Res.*, *107*(B3), 2056, doi:10.1029/2001JB000486.

Emmanuel, S., and B. Berkowitz (2006), Suppression and stimulation of seafloor hydrothermal convection by exothermic mineral hydration, *Earth Planet. Sci. Lett.*, *243*, 657–668, doi:10.1016/j.epsl.2006.01.028.

Escartín, J., G. Hirth and B. Evans (1997), Effects of serpentinization on the lithospheric strength and the style of normal faulting at slow-spreading ridges, *Earth Planet. Sci. Lett.*, *151*, 181–189, doi:10.1016/S0012-821X(97)81847-X.

Escartín, J., G. Hirth and B. Evans (2001), Strength of slightly serpentinized peridotites: Implications for the tectonics of oceanic lithosphere, *Geology*, *29*, 1023–1026, doi:10.1130/0091-7613(2001)029<1023:SOSSPI>2.0.CO;2.

Evans, B. W. (2008), Control of the products of serpentinization by the $Fe^{2+}Mg_{-1}$ exchange potential of olivine and orthopyroxene, *J. Petrol.*, *49*, 1873–1887, doi:10.1093/petrology/egn050.

Fyfe, W. S. (1974), Heats of chemical reactions and submarine heat production, *Geophys. J. Int.*, *37*, 213–215, doi:10.1111/j.1365-246X.1974.tb02454.x.

Heider, F., D. J. Dunlop, and N. Sugiura (1987), Magnetic properties of hydrothermally recrystallized magnetite crystals, *Science*, *236*, 1287–1290, doi:10.1126/science.236.4806.1287.

Heider, F., A. Zitzelsberger, and K. Fabian (1996), Magnetic susceptibility and remanent coercive force in grown magnetite crystals from 0.1 μm to 6 mm, *Phys. Earth Planet. Inter.*, *93*, 239–256, doi:10.1016/0031-9201(95)03071-9.

Hu, M., R.-P. Ji, and J.-S. Jiang (2010), Hydrothermal synthesis of magnetite crystals: From sheet to pseudo-octahedron, *Mater. Res. Bull.*, *45*, 1811–1815, doi:10.1016/j.materresbull.2010.09.023.

Hyndman, R. D., and S. M. Peacock (2003), Serpentinization of the forearc mantle, *Earth Planet. Sci. Lett.*, *212*, 417–432, doi:10.1016/S0012-821X(03)00263-2.

Johnson, J. W., E. H. Oelkers, and H. C. Helgeson (1992), SUPCRT92: A software package for calculating the standard molal thermodynamic properties of minerals, gases, aqueous species, and reactions from 1 to 5000 bar and 0 to 1000°C, *Comput. Geosci.*, *18*, 899–947, doi:10.1016/0098-3004(92)90029-Q.

Klein, F., W. Bach, N. Jöns, T. McCollom, B. Moskowitz, and T. Berquo (2009), Iron partitioning and hydrogen generation during serpentinization of abyssal peridotites from 15°N on the Mid-Atlantic Ridge, *Geochim. Cosmochim. Acta*, *73*, 6868–6893, doi:10.1016/j.gca.2009.08.021.

Krammer, K. (1990), Rock magnetic properties and opaque mineralogy of selected samples from Hole 670A, *Proc. Ocean Drill. Program, Sci. Results*, *106/109*, 269–273.

Liu, Q., Q. Zeng, J. Zheng, T. Yang, N. Qiu, Z. Liu, Y. Luo, and Z. Jin (2010), Magnetic properties of serpentinized garnet peridotites from the CCSD main hole in the Sulu ultrahigh-pressure metamorphic belt, eastern China, *J. Geophys. Res.*, *115*, B06104, doi:10.1029/2009JB000814.

Marcaillou, C., M. Muñoz, O. Vidal, T. Parra, and M. Harfouche (2011), Mineralogical evidence for H_2 degassing during serpentinization at 300°C/300 bar, *Earth Planet. Sci. Lett.*, *303*, 281–290, doi:10.1016/j.epsl.2011.01.006.

Martin, B., and W. S. Fyfe (1970), Some experimental and theoretical observations on the kinetics of hydration reactions with particular reference to serpentinization, *Chem. Geol.*, *6*, 185–202, doi:10.1016/0009-2541(70)90018-5.

McCollom, T. M., and W. Bach (2009), Thermodynamic constraints on hydrogen generation during serpentinization of ultramafic rocks, *Geochim. Cosmochim. Acta*, *73*, 856–875, doi:10.1016/j.gca.2008.10.032.

Moody, J. B. (1976), An experimental study on the serpentinization of iron-bearing olivines, *Can. Mineral.*, *14*, 462–478.

Nazarova, K. A. (1994), Serpentinized peridotites as a possible source for oceanic magnetic anomalies, *Mar. Geophys. Res.*, *16*, 455–462, doi:10.1007/BF01270519.

Neal, C., and G. Stanger (1983), Hydrogen generation from mantle source rocks in Oman, *Earth Planet. Sci. Lett.*, *66*, 315–320, doi:10.1016/0012-821X(83)90144-9.

Néel, L. (1953), Thermoremanent magnetization of fine powders, *Rev. Mod. Phys.*, *25*, 293–295, doi:10.1103/RevModPhys.25.293.

O'Reilly, W. (1984), *Rock and Mineral Magnetism*, 220 pp., Blackie, New York.

Oufi, O., M. Cannat, and H. Horen (2002), Magnetic properties of variably serpentinized abyssal peridotites, *J. Geophys. Res.*, *107*(B5), 2095, doi:10.1029/2001JB000549.

Özdemir, Ö., and D. J. Dunlop (1992), Domain structure observations in biotite and hornblendes, *Eos Trans. AGU*, *73*(14), *Spring Meet. Suppl.*, 93.

Rahman, A. A., A. D. Duncan, and L. G. Parry (1973), Magnetization of multidomain magnetite particles, *Riv. Ital. Geofis.*, *22*, 259–266.

Rasmussen, M. G., B. W. Evans, and S. M. Kuehner (1998), Low-temperature fayalite, greenalite, and minnesotaite from the Overlook gold deposit, Washington; phase relations in the system FeO-SiO_2-H_2O, *Can. Mineral.*, *36*, 147–162.

Seyfried, W. E., Jr., D. I. Foustoukos, and Q. Fu (2007), Redox evolution and mass transfer during serpentinization: An experimental and theoretical study at 200°C, 500 bar with implications for ultramafic-hosted hydrothermal systems at Mid-Ocean Ridges, *Geochim. Cosmochim. Acta*, *71*, 3872–3886, doi:10.1016/j.gca.2007.05.015.

Stoner, E. C., and E. P. Wohlfarth (1948), A mechanism of magnetic hysteresis in heterogeneous alloys, *Philos. Trans. R. Soc. London, Ser. A*, *240*, 599–642, doi:10.1098/rsta.1948.0007.

Tauxe, L. (1998), *Paleomagnetic Principles and Practice*, Kluwer Acad., Dordrecht, Netherlands.

Toft, P. B., J. Arkani-Hamed, and S. E. Haggerty (1990), The effects of serpentinization on density and magnetic susceptibility: A petrophysical model, *Phys. Earth Planet. Inter.*, *65*, 137–157, doi:10.1016/0031-9201(90)90082-9.

F. Brunet and B. Malvoisin, Maison des Géosciences, ISTerre, Université de Grenoble 1, CNRS, BP 53, F-38041 Grenoble, France. (benjamin.malvoisin@ujf-grenoble.fr)

J. Carlut, Laboratoire de Géosciences Marines, Institut de Physique du Globe de Paris, CNRS, 1 rue Jussieu, F-75238 Paris CEDEX 5, France.